Turkish Journal of Engineering & Environmental Sciences

http://journals.tubitak.gov.tr/engineering/

Research Article

Turkish J Eng Env Sci
(2014) 38: 293 – 307

doi:10.3906/muh-1310-2

Theoretical and experimental investigation of the performance of back-pass solar air heaters

Zeliha Deniz ALTA[1], Nuri ÇAĞLAYAN[1], İbrahim ATMACA[2], Can ERTEKİN[1,*]

[1]Department of Farm Machinery and Technologies Engineering, Faculty of Agriculture, Akdeniz University, Antalya, Turkey

[2]Department of Mechanical Engineering, Faculty of Engineering, Akdeniz University, Antalya, Turkey

Received: 08.10.2013 • **Accepted/Published Online:** 24.04.2015 • **Printed:** 30.06.2015

Abstract: This paper presents a study dealing with the experimental and theoretical analysis of a flat plate solar air heater. The air collectors were tested experimentally for the tilt angle of 35° and 2 m s^{-1} air velocity, and ambient temperature, inlet temperature, outlet temperature, absorber plate temperature, bottom plate temperature, solar radiation, air velocity, and airflow velocity from the duct were measured. The outlet air temperature and energy and exergy efficiencies of the collector were calculated theoretically. The results showed that the collector has the maximum mean outlet temperature for the airflow velocity of 1 m s^{-1}, duct height of 0.001 m, triple glass cover, and length of 3 m; the maximum mean energy efficiency for the airflow velocity of 4 m s^{-1}, duct height of 0.04 m, triple glass cover, and length of 1 m; and the maximum mean exergy efficiency for the airflow velocity of 1 m s^{-1}, duct height of 0.005 m, triple glass cover, and length of 3 m. This study demonstrated the superiority of exergy analysis over energy analysis before the decision regarding design parameters.

Key words: Solar air heater, air collector, absorber plate, energy analysis, exergy analysis

1. Introduction

The thermal efficiency of a solar collector is the major requirement for the prediction of thermal performance of the complete solar system [1]. It has been found to be generally poor for solar air heaters because of their inherently low heat transfer capacity between the absorber plate and air flowing in the duct [2]. As the performance is poor and it is simple in construction, there is a need for the determination of the domain of optimum system and operating parameters so that the system can be operated at its highest capabilities [3]. To improve the thermal performance of flat plate solar air heaters, it is essential to increase the temperature of the air leaving the collector by optimizing the main dimensions of the collector as air channel depth with respect to its length and width or providing artificial roughness on the underside of the absorber plate [4].

A method was established by Torres-Reyes et al. to determine the optimum temperature and path flow length of a solar collector [4,5]. Design formulas for different air duct and absorber plate arrangements were obtained. Hegazy presented a remarkably simple criterion for determining the optimum channel geometry that effectively maximizes the useful energy from collectors designed to heat a fixed mass rate of airflow [2]. For variable flow operation, however, a depth-to-length ratio of 0.0025 is recommended as optimal for the collector with air flowing between the absorber plate and the back panel. The optimal channel depths for the collector

*Correspondence: ertekin@akdeniz.edu.tr

with air flowing between the absorber plate and the cover glazing and the collector with two air channels above and below the absorber plate with black-painted absorber are suggested as 10 mm and no less than 20 mm. Smaller channel depth results in significant friction loss, while larger depth increases heat loss. In the collector, airflows in two channels, the depth ratio of up channel to down channel should be no less than 1. Gupta and Kaushik also determined the optimum aspect ratio (length to width ratio of the absorber plate) and optimum duct depth (the distance between the absorber and the bottom plates) for maximum exergy delivery [6]. Luna et al. studied different modelling approaches for a solar air collector to use a low number of variables and equations in design [7]. Different types of natural circulation air heating solar collectors were designed, constructed, and analyzed for their performance by Koyuncu [8]. A single covered and front-pass type collector was proposed because of its higher efficiency. Thermal performance was obtained by Varun for different Reynolds numbers, plate emissivities, tilt angles, and number of glass covers by genetic algorithm [3]. A computer program based on the proposed optimization was developed in MATLAB to obtain maximum thermal performance of a flat plate solar air heater. Dhiman et al. presented a mathematical model for a parallel flow solar air heater with porous media and made a theoretical solution procedure of the energy equations [9]. They predicted the various temperatures and thermal performance of a parallel flow packed bed solar air heater by using a computer code in MATLAB. Karwa and Chauhan studied the thermohydraulic performance of a roughened duct solar air heater with 60° "V" down discrete rib roughness on the airflow side of the absorber plate [10]. A detailed investigation was carried out using a mathematical model. The results showed that roughened duct solar air heaters provide a significant performance advantage over smooth duct air heaters. Varol and Öztop carried out a theoretical study to investigate natural convection heat transfer and flow field inside collectors with flat and wavy absorber plates [11]. CFDRC (Computational Fluid Dynamics Research Corporation) commercial software was used to simulate the laminar flow and thermal field. It was observed that flow and thermal fields are affected by the shape of the enclosure.

The aim of the present study was to investigate the effects of different values of the parameters airflow velocity, air flow duct height, the number of glass covers, and the length of the collector by using of the algorithm with time and cost savings. The differences between this study and the similar published works are solving the algorithm with the most common relevant formula using FORTRAN software for defined collector parameters and evaluating the system taking into account the exergy efficiencies as well as energy efficiencies. For this purpose, a back-pass solar air heater was designed and an experimental study was conducted for 2.0 m s^{-1} air velocity. The system was also analyzed by using a simulation run with the developed algorithm and both results were compared. After validation, optimum design parameters for the maximum thermal and effective efficiencies of the collector were calculated with the simulation program. Optimum airflow duct height, airflow velocity, number of glass covers, and length of the collector were investigated to obtain maximum outlet temperature and energy or exergy efficiency. The friction factor was neglected because of the absence of roughness on the underside of the absorber plate and inside the duct.

2. Theoretical analysis of back-pass solar air heaters

In this type of collector, the absorber plate is placed behind the glass cover with a gap filled with static air for the glass cover and the flow of air happens between the bottom surface of the absorber and the upper surface of insulation (Figure 1). The basic idea is that the air is heated as it moves upwards behind the heated solar absorber.

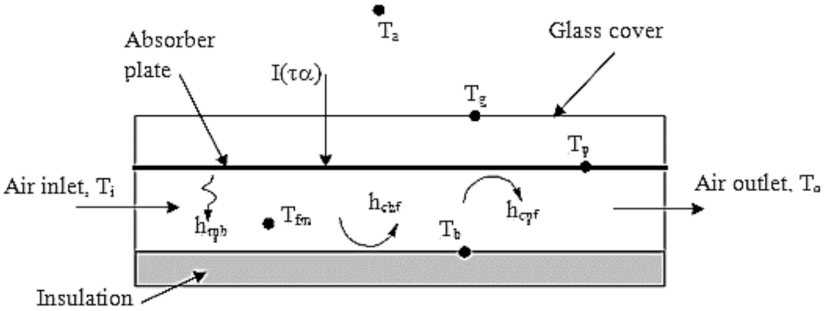

Figure 1. Heat balance of a back-pass solar air heater.

The air properties can be calculated by the following equations [12]:

$$C_p = 975.2 + 0.12468\,T_i + 3.3132 \times 10^{-6}\,T_i^2 \tag{1}$$

$$\mu = 4.314 \times 10^{-7} + 6.779 \times 10^{-8}\,T_i - 2.39 \times 10^{-11}\,T_i^2 \tag{2}$$

$$\lambda = 0.003954 + 7.72083 \times 10^{-5}\,T_i - 1.60822 \times 10^{-8}\,T_i^2 \tag{3}$$

$$\rho = 1.9049 - 3.04328 \times 10^{-3}\,T_i - 1.3889 \times 10^{-6}\,T_i^2 \tag{4}$$

Wind heat transfer coefficient is calculated as below, where V_r is wind velocity:

$$h_w = 5.7 + 3.8V_r \quad \left(0 \le V_r \le 5\,m\,s^{-1}\right) \tag{5}$$

The top heat loss coefficient is [8]

$$U_t = \left[\frac{N}{\left(\frac{C}{T_{pm}}\right)\left(\frac{(T_{pm}-T_a)}{(N+f)^e}\right)} + \frac{1}{h_w}\right]^{-1} + \left[\frac{\sigma\,(T_{pm}+T_a)\,\left(T_{pm}^2+T_a^2\right)}{\frac{1}{\varepsilon_p+0.00591\,N\,h_w} + \frac{2\,N+f\,-1+0.133\,\varepsilon_p}{\varepsilon_g} - N}\right], \tag{6}$$

where $N$is number of transparent covers; C is a coefficient related to title angle; f is a coefficient related to wind heat transfer coefficient, emissivity of the absorber plate, and the number of transparent cover; and e is a coefficient related to the temperature of the absorber plate.

$$C = 520\left(1 - 0.000051\,\beta^2\right) \tag{7}$$

$$f = (1 + 0.089\,h_w - 0.1166\,h_w\,\varepsilon_p)\,(1 + 0.07866\,N) \tag{8}$$

$$e = 0.430\left[1 - \left(\frac{100}{T_{pm}}\right)\right] \tag{9}$$

β is the heater tilt angle, T_{pm} is temperature of the absorbing plate, ε_p is emissivity of the absorbing plate, and ε_g is emissivity of the transparent cover.

The bottom and edge heat loss coefficients are as follows, respectively:

$$U_b = \frac{\lambda}{t_b} \tag{10}$$

$$U_e = \left(\frac{\lambda\, p\, h_e}{t_e}\right)\left(\frac{1}{A_c}\right), \tag{11}$$

where λ is thermal conductivity of the insulation material, t_b and t_e are the thickness of the insulation material of the bottom and edge, respectively, p is the perimeter of the heater, and h_e is the heater height.

The overall heat loss coefficient is the sum of top, bottom, and edge heat loss coefficients:

$$U_L = U_t + U_b + U_e \tag{12}$$

The Reynolds number of the airflow is

$$Re_{Dh} = \frac{\rho V D_h}{\mu} \tag{13}$$

through a particular channel of hydraulic diameter:

$$D_h = \frac{4WD}{2D + 2W} \tag{14}$$

The relative heat transfer coefficients between the absorber plate and the bottom plate are calculated by the following equation:

$$h_{rpb} = \sigma\left(T_p - T_b\right)\left(T_p^2 + T_b^2\right)/[(1/\varepsilon_p) + (1/\varepsilon_b) - 1] \tag{15}$$

The heat transfer coefficients of the flow channel between the upper and lower plates are considered equal [2]:

$$h_{cpf} = h_{cbf} = \frac{\lambda}{D_h}\left[0.0158Re_{Dh}^{0.8} + (0.00181Re_{Dh} + 2.92)\ exp\left(-0.03795L/D_h\right)\right] \tag{16}$$

The Nusselt number for $0.5 < Pr < 2000$ and $3000 < Re < 5 \times 10^6$ is [12]

$$Nu = \frac{(f/8)\ (Re - 1000)\ Pr}{1 + 12.7\,(f/8)^{1/2}\left(Pr^{2/3} - 1\right)} \tag{17}$$

where the friction factor is [12]

$$f = \left(0.790 \ln Re - 1.64\right)^{-2}$$

$$\left(3000 < Re < 5 \times 10^6\right) \tag{18}$$

The collector efficiency factor $F\prime$ is [13,14]

$$F' = \left[1 + \frac{U_L}{h_{cpf} + [(1/h_{cpf}) + (1/h_{rpb})]^{-1}}\right] \tag{19}$$

The collector flow factor is a function of the single variable, dimensionless collector capacitance rate $\dot{m}c_p/A_c\,U_L\,F'$ and it is convenient to define F'' as the ratio of F_R and $F\prime$. Thus,

$$F'' = \frac{F_R}{F'} = \frac{\dot{m}\,c_p}{A_c\,U_L\,F'}\left[1 - exp\left(-\frac{A_c\,U_L\,F'}{\dot{m}\,c_p}\right)\right], \tag{20}$$

where c_p is the specific heat of air at constant pressure. The collector heat removal factor can be expressed as

$$F_R = F'F'' \tag{21}$$

The collected heat is transferred to the air flowing through the air heater duct. Thus the useful heat gain can be expressed as [5,14]

$$Q_u = A_c\, F_R \left[G_T\ (\tau\alpha) - U_L\ (T_i - T_a)\right], \tag{22}$$

where $\tau\alpha$ is the transmittance-absorptance product, G_T is the solar radiation on the collector plane, T_i is the inlet air temperature, and T_a is the ambient air temperature. T_{fm} is the mean temperature of air in the solar air heater duct, $(T_o + T_i)/2$ or calculated as below [14]:

$$T_{fm} = T_i + (Q_u/A_c)/(U_L F_R)\,(1 - F_R/F') \tag{23}$$

The mean plate temperature will always be greater than the mean fluid temperature due to the heat transfer resistance between the absorbing surface and the fluid. This temperature difference is usually small for liquid systems but may be significant for air systems [14].

The mean plate temperature can be found by

$$T_{pm} = T_i + (Q_u/A_c)/(U_L F_R)\,(1 - F_R) \tag{24}$$

The outlet temperature is

$$T_o = T_i + (Q_u/\dot{m}\, c_p) \tag{25}$$

Energy efficiency of the collector is calculated using heat gain and solar radiation, using the equation

$$\eta_I = \frac{Q_u}{A_c\, G_T} \tag{26}$$

Exergy efficiency of the collector is calculated as follows [15]:

$$\eta_{II} = 1 - \frac{I}{\left[1 - \frac{T_a}{T_s}\right] Q_s}, \tag{27}$$

where Q_s is solar energy absorbed by the collector absorber surface, T_s is the apparent sun temperature (which is approximately set equal to 6000 K), and I is the irreversibility, expressed by

$$Q_s = G_T\,(\tau\alpha)\ A_c \tag{28}$$

$$I = \left(1 - \frac{T_a}{T_s}\right) Q_s - \dot{m}\left[(h_{out} - h_{in}) - T_a(S_{out} - S_{in})\right] \tag{29}$$

There are two main sources of entropy generation in a solar air collector, one due to the friction of passing fluid and the other due to the thermal heat transfer or temperature change of air. The following assumptions are used to derive the exergy equations [16]:

1. The process is steady state and steady flow,
2. The potential and kinetic energies are negligible,
3. Air is an ideal gas and so its specific heat is constant,
4. The humidity of air is negligible.

3. Experimental procedures

In the experimental study, a back-pass type flat plate solar air heater was designed, fabricated, and installed. The schematic diagram of the experimental set-up is shown in Figure 1. Single glazing was chosen in order to maximize the radiation impact on the absorber plate. The heater was insulated from the back and sides using glass wool as an insulating material with thickness of 0.05 m to minimize heat losses. The gap between the absorber plate and bottom plate is 0.043 m. A matte black painted sheet of copper with thickness of 0.001 m was used as an absorber plate. The air was provided by a radial fan with a maximum 0.41 m^3 s^{-1} mass flow rate. The flow rate could be controlled by the flap setting on the fan. The collectors were located with 35° tilt angles toward to the south. The parameters of the designed collector are summarized in the Table.

Table. Main properties of the designed collector.

Collector parameters	Value
Type	Black paint flat plate
Glazing	Single glass
Agent fluid in flow ducts	Air
With of the duct, W	0.9 m
Collector side wall height, h_e	0.1 m
Air flow duct height, D	43 mm
Length of the collector, L	1.9 m
Emissivity of the glass cover, ε_g	0.85
Emissivity of the absorber plate, ε_p	0.95
Emissivity of the bottom plate, ε_b	0.95
Tilt angle, β	35°
Insulation thicknesses, t_b, t_e	50 mm
Thermal conductivity of insulation, λ	0.043 W m^{-1} K^{-1}

Inlet and outlet air temperature, ambient temperature, plate temperature, and airflow temperature in the duct were measured using 25 K-type thermocouples. Figures 2a and 2b show the location of 11 thermocouples affixed on the absorber plate to measure the plate temperature. A total of 11 thermocouples were affixed on the bottom plate to measure the mean flow temperatures; one thermocouple was also installed in the inlet pipe, one in the outlet pipe, and one for ambient temperatures.

It is possible to arrange a number of thermocouples such that their combined output represents an average of their temperatures. An operationally convenient system is to connect all the thermocouples in parallel (Figure 3).

Wind speed was measured by using a cup anemometer (Delta-T A100 R model, accuracy 1% ± 0.1 m s^{-1}). The instrument was installed in the vicinity of the collector at a height of not less than the height of the collector. A flow meter [Testo 405, accuracies ± (0.1 m s^{-1} ±5% of m.v.) at 0–2 m s^{-1} and ± (0.3 m s^{-1} ±5% of m.v.) at 2.01–10 m s^{-1}] was used to measure the velocity of flowing air at the inlet of the collector in a vertical position. The global solar radiation incident on the collector was measured using a solar meter type Delta-T ES2 sensor (accuracy ±3% at 20 °C). The solar meter was installed at the level of the glass cover of the solar air heater. Each set of experiments was conducted during the steady-state period at 5 min intervals and logged by Delta-T Data Logger. The locations of some sensors are shown in Figures 4a–4d. The experiments were carried out between at 0900 and 1700 on a weekday. Total uncertainty for collector efficiency

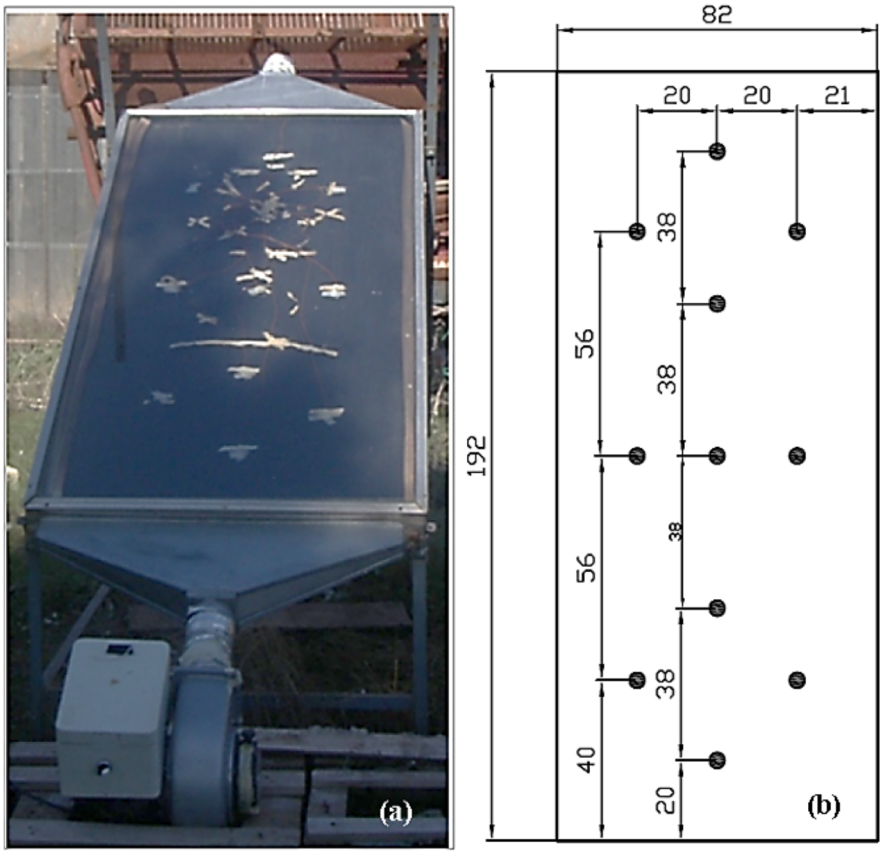

Figure 2. Solar air heater (a) and locations of the thermocouples on the absorber plate (dimensions are in cm) (b).

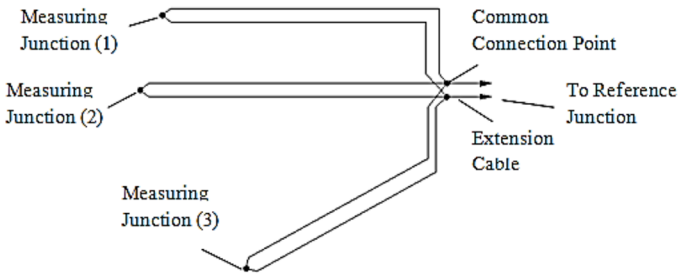

Figure 3. Junction of thermocouples for average temperature.

can be written as follows:

$$w_\eta = \left[\left(\frac{\partial \eta}{\partial \dot{m}} w_{\dot{m}} \right)^2 + \left(\frac{\partial \eta}{\partial T_{out}} w_{T_{out}} \right)^2 + \left(\frac{\partial \eta}{\partial T_{in}} w_{T_{in}} \right)^2 + \left(\frac{\partial \eta}{\partial T_a} w_{T_a} \right)^2 + \left(\frac{\partial \eta}{\partial G_T} w_{G_T} \right)^2 + \left(\frac{\partial \eta}{\partial V_r} w_{V_r} \right)^2 \right]^{1/2} \quad (30)$$

The total uncertainty for the efficiency of the collector was estimated by Eq. (30) and found as 3%.

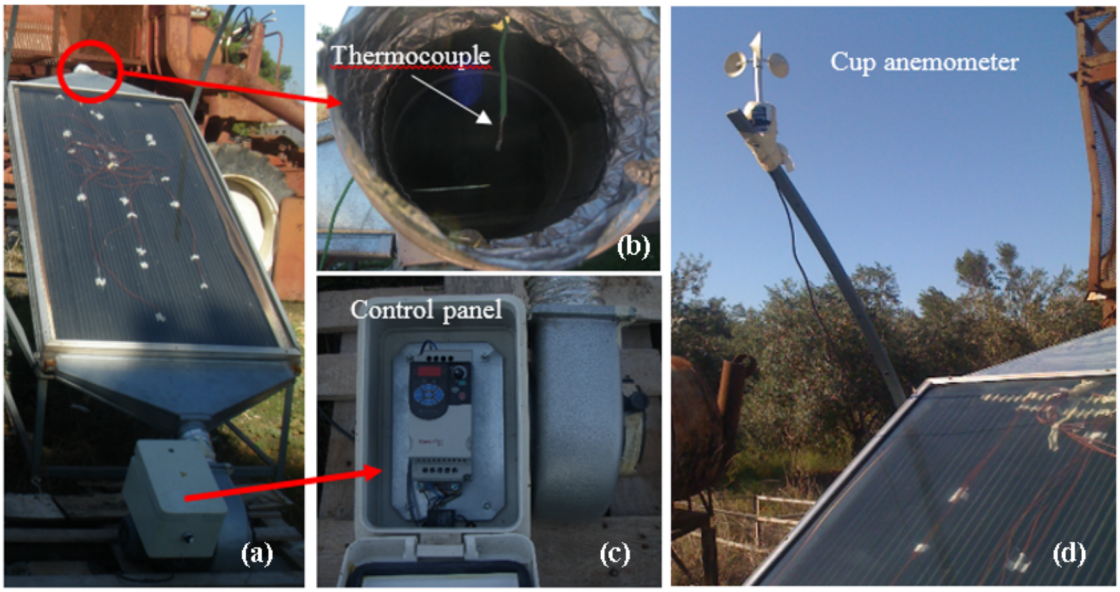

Figure 4. Solar air heater (a), locations of thermocouple for measuring of outlet air temperature (b), the speed control panel of fan (c), and the cup anemometer to measure wind speed (d).

4. Simulation

A suitable algorithm was prepared in FORTRAN language for the solution of energy equations for flat plate solar air heaters. Eqs. (1)–(30) were solved by following the iterative process presented in Figure 5. The iteration was terminated when the difference between the estimated and calculated plate temperature was less than 1 K. The result of the mathematical model used here was validated by the results of the experimental study. The following climatic parameters were taken from measured values: intensity of solar radiation, ambient temperature, and wind speed. The following design parameters were determined: the size of the collector, size of the duct, thickness of the insulations, and number of glass covers. The operational parameter, the mass flow rate of the air flowing in the duct, was also calculated from the measured velocity of the forced air.

The algorithm was initiated reading the climatic, design, and operational parameters and assuming the plate temperature. Collector efficiency was calculated using initial values, heat losses, heat transfer coefficients, useful heat gain, and outlet, mean plate, and flow temperatures.

5. Results and discussion

Figure 6 presents solar radiation, and ambient, inlet, and outlet temperatures versus experiment time for a typical day, 13 August. It seems that inlet and outlet air temperatures increase with solar radiation and the maximum values are at midday. The maximum difference between inlet and outlet air temperatures is 36.1 K.

The results of the comparisons of the outlet temperatures obtained from the experiment and theoretical calculations by using simulation for the airflow velocities of 2.0 m s^{-1} showed that the simulation results are very close to the experimental data. The differences in the outlet temperatures of simulation and experimental results varied between 1.6% and 6.9%. These differences could have occurred from the accuracy of the measurements, possible air leakages from the collector, and the assumptions in the equations used for simulation etc.

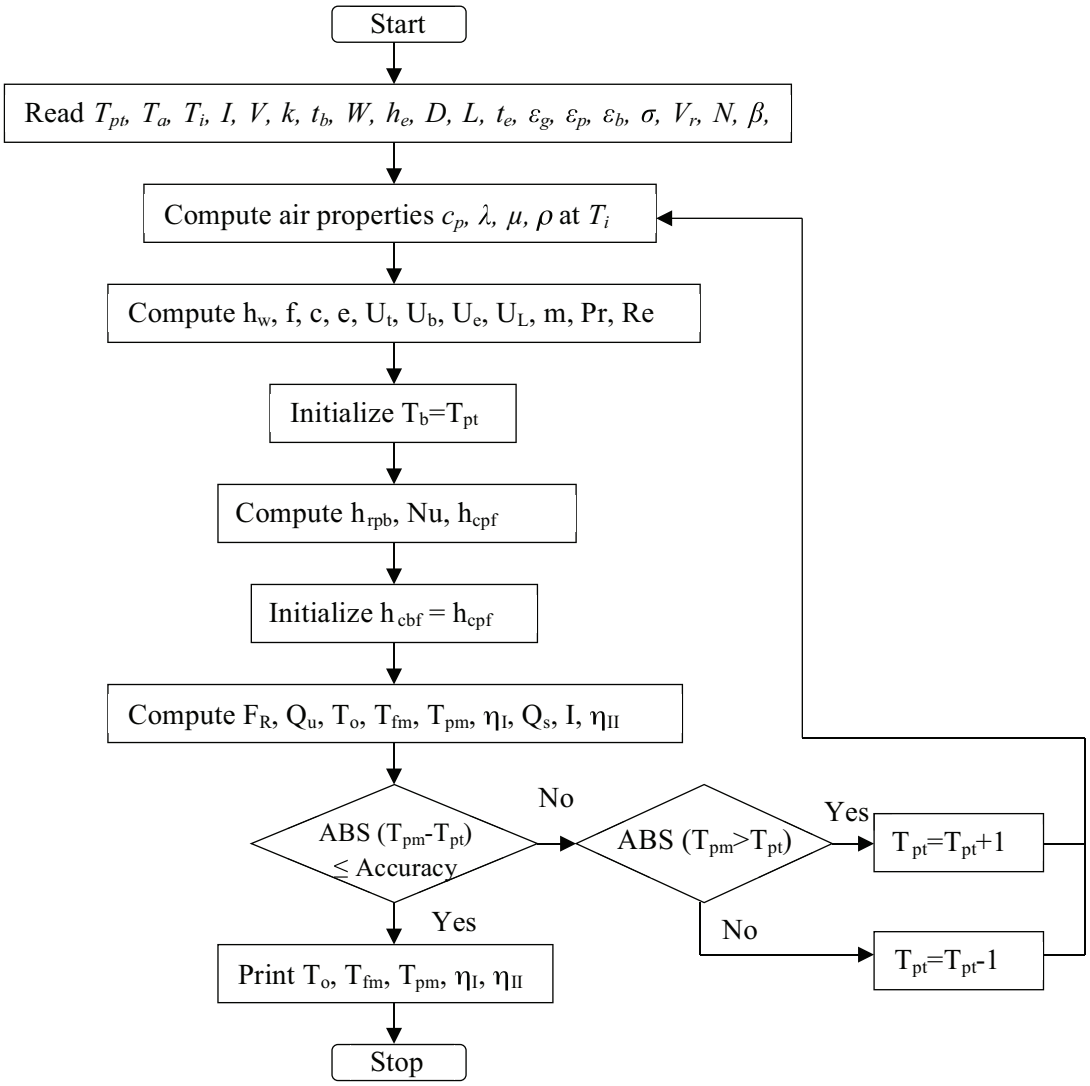

Figure 5. Flow chart for algorithm.

As the next step of this study, the effects of the dimensions of the design parameters air velocity, flow duct height, number of glass covers, and length of the collector on the outlet temperatures and the collector efficiencies were investigated theoretically by using simulation with the margin of error determined above. The initial data were accepted as the data for the air velocity of 2.0 m s^{-1} and the given design and operational parameters (L = 1.9 m; h_e = 10 mm; W = 0.9 m; ε_p = 0.95; ε_b = 0.95; ε_p = 0.85; β = 35°; T_a = 308.8, 313.9, 310.9, 310.9, 310.0, 308.9, 309.6, 309.7, 304.9; T_i = 312.3, 317.3, 318.7, 316.5, 315.0, 313.4, 313.2, 313.2, 306.7; I = 592, 819, 980, 1093, 1085, 990, 810, 607, 388; and V_r = 1.25, 1.12, 1.84, 2.77, 2.67, 3.13, 2.98, 2.35, 1.92).

Outlet temperature, and energy and exergy efficiencies were investigated for different airflow velocities, i.e. 1.0, 2.0, 3.0, and 4.0 m s^{-1}. The results are shown in Figures 7–9. Outlet temperature decreased but energy efficiency increased as the air velocity increased. Exergy efficiency had its maximum values in the air velocity of 1 m s^{-1} but then decreased depending on the velocity increases. Reynolds number was about 3323–3637 for 1 m s^{-1} air velocity, 6646–7274 for 2 m s^{-1} air velocity, 9969–10,912 for 3 m s^{-1} air velocity,

and 13,293–13,953 for 4 m s^{-1} air velocity. As seen in the Reynolds numbers, the analysis was conducted for airflow with turbulence.

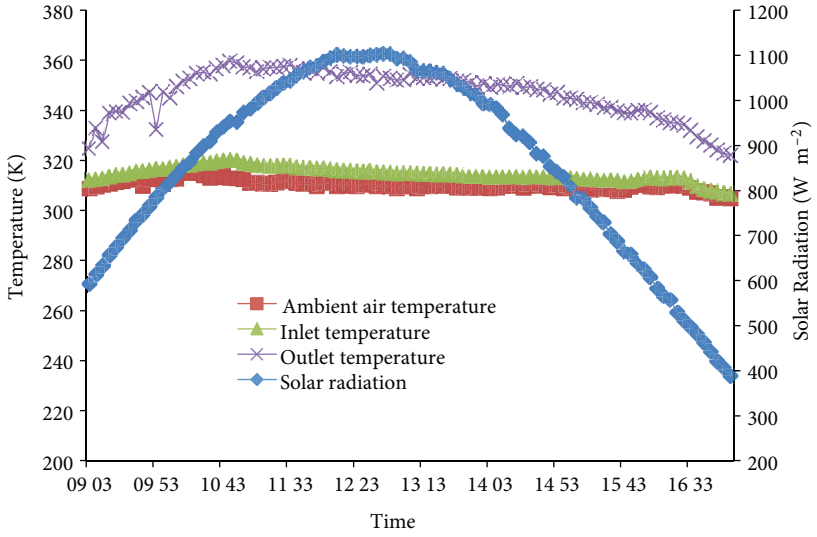

Figure 6. Solar radiation, and ambient, inlet, and outlet air temperature for the solar air heater on a typical day.

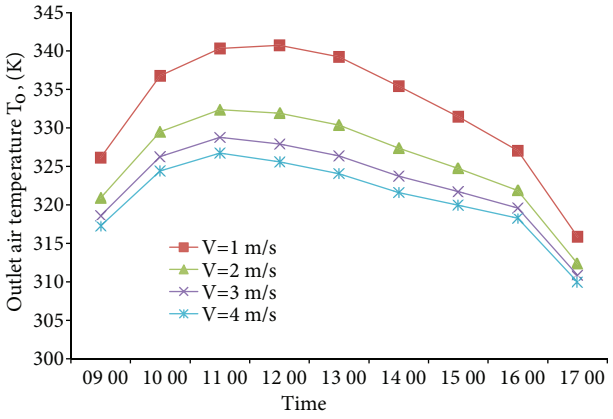

Figure 7. Variation in outlet temperature for different air flow velocity values (L = 1.9 m, h_e = 0.01 m, W = 0.9 m, D = 0.043 m, N = 1).

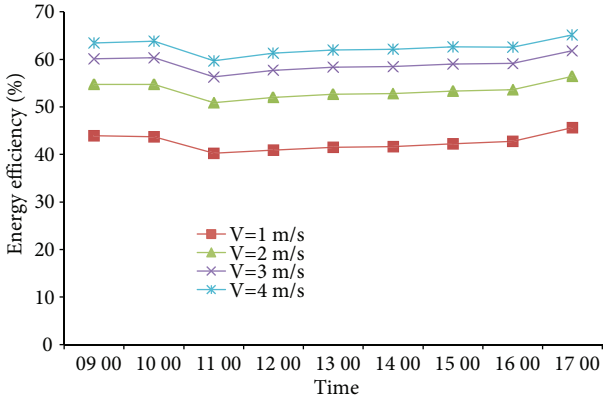

Figure 8. Variation in energy efficiency for different air flow velocity values (L = 1.9 m, h_e = 0.01 m, W = 0.9 m, D = 0.043 m, N = 1).

The maximum outlet temperature was 340.7 K for 1 m s^{-1} air velocity at 1200 hours. Mean outlet temperatures were 332.5, 325.7, 322.6, and 320.8 K for the airflow velocity of 1, 2, 3, and 4 m s^{-1}, respectively. The collector had the maximum mean outlet temperature for the airflow velocity of 1 m s^{-1}.

The maximum energy efficiency was 65.1% for 4 m s^{-1} air velocity at 1700 hours. Mean energy efficiencies were 42.5%, 53.4%, 59.0%, and 62.5% for the airflow velocity of 1, 2, 3, and 4 m s^{-1}, respectively. The collector had the maximum mean energy efficiency for the airflow velocity of 4 m s^{-1}.

The maximum exergy efficiency was 2.8% for 2 m s^{-1} air velocity at 1100 hours. Mean exergy efficiencies were 2.17%, 2.08%, 1.96%, and 1.87% for the airflow velocity of 1, 2, 3, and 4 m s^{-1}, respectively. The collector had the maximum mean exergy efficiency for the airflow velocity of 1 m s^{-1}.

Outlet temperature, and energy and exergy efficiencies were also investigated for different dimensions of depth in duct, i.e. 0.01, 0.1, 0.5, 1, 2, 3, and 4 cm. The results are shown in Figures 10–12. Outlet temperature decreased for the dimension of duct height more or less than 0.1 cm. Energy efficiency increased with the increase in duct height. Exergy efficiency increased but began to decrease gradually after the height of the duct was more than 0.5 cm.

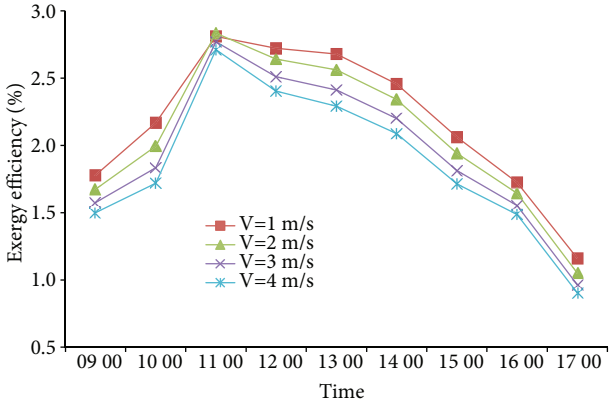

Figure 9. Variation in exergy efficiency for different air flow velocity values (L = 1.9 m, h_e = 0.01 m, W = 0.9 m, D = 0.043 m, N = 1).

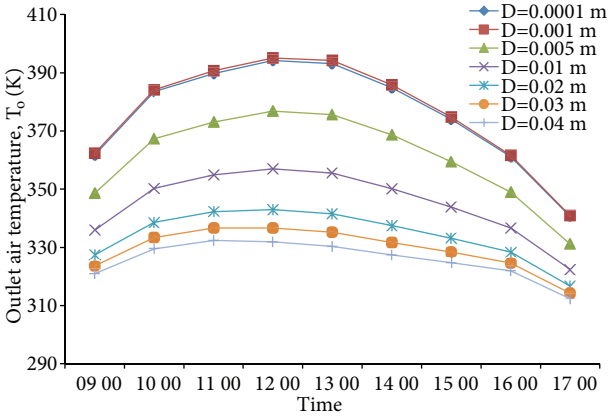

Figure 10. Variation in outlet temperature for different dimensions of duct height velocity (L = 1.9 m, h_e = 0.01 m, W = 0.9 m, V = 2 m s^{-1}, N = 1).

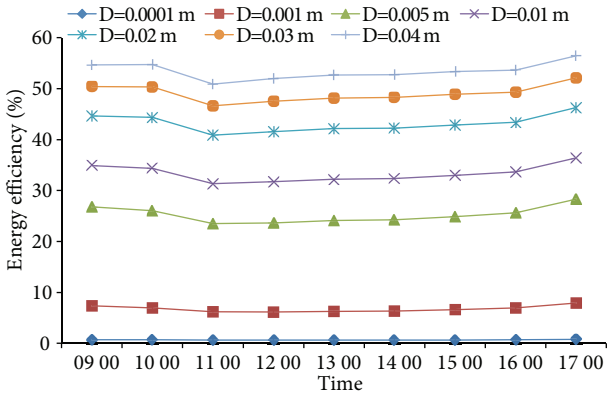

Figure 11. Variation in energy efficiency for different dimensions of duct height (L = 1.9 m, h_e = 0.01 m, W = 0.9 m, V = 2 m s^{-1}, N = 1).

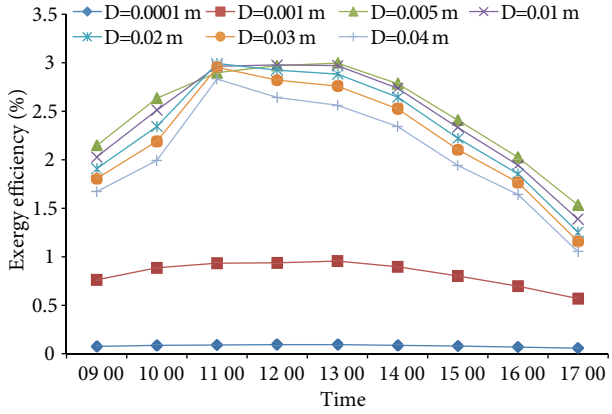

Figure 12. Variation in exergy efficiency for different dimensions of duct height (L = 1.9 m, h_e = 0.01 m, W = 0.9 m, V = 2 m s^{-1}, N = 1).

The maximum outlet temperature was 395.0 K for the duct height of 0.001 m at 1200 hours. Mean outlet temperatures were 375.8, 376.6, 361.0, 345.1, 334.2, 329.3, and 325.7 K for the duct height of 0.0001, 0.001, 0.005, 0.01, 0.02, 0.03, and 0.04 m, respectively. The collector had the maximum mean outlet temperature for the duct height of 0.001 m.

The maximum energy efficiency was 56.4% for 0.04 m duct height at 1700 hours. Mean energy efficiency was 0.6%, 6.7%, 25.2%, 33.3%, 43.1%, 49.0%, and 53.4% for the duct height of 0.0001, 0.001, 0.005, 0.01, 0.02, 0.03, and 0.04 m, respectively. The collector had the maximum mean energy efficiency for the duct height of 0.04 m.

The maximum exergy efficiency was 2.99% for 0.005 m duct height at 1300 hours. Mean exergy efficiency was 0.08%, 0.83%, 2.49%, 2.43%, 2.34%, 2.23%, and 2.08% for the duct height of 0.0001, 0.001, 0.005, 0.01, 0.02, 0.03, and 0.04 m, respectively. The collector had the maximum mean exergy efficiency for the duct height of 0.005 m.

The result found from exergy analysis for the optimum height of the duct of 0.005 m or the depth-to-length ratio of 0.0025 for the designed collector is appropriate with the optimum channel geometry that Hegazy recommended to maximize the useful energy.

Outlet temperature, and energy and exergy efficiencies were investigated for different numbers of glass covers. The results are shown in Figures 13–15. All of them increased with the increase in the number of glass covers.

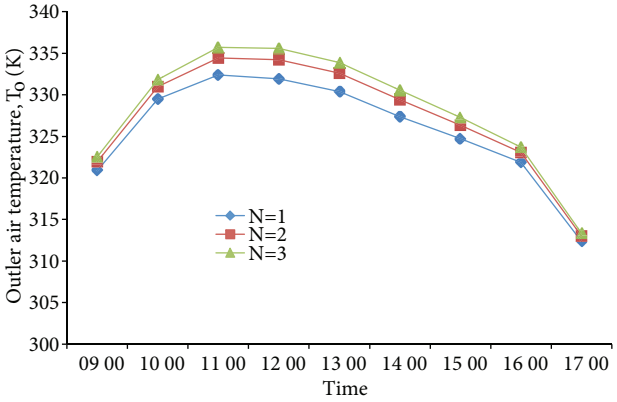

Figure 13. Variation in outlet temperature for different numbers of glass covers (L = 1.9 m, h_e = 0.01 m, W = 0.9 m, V = 2 m s^{-1}, D = 0.043 m).

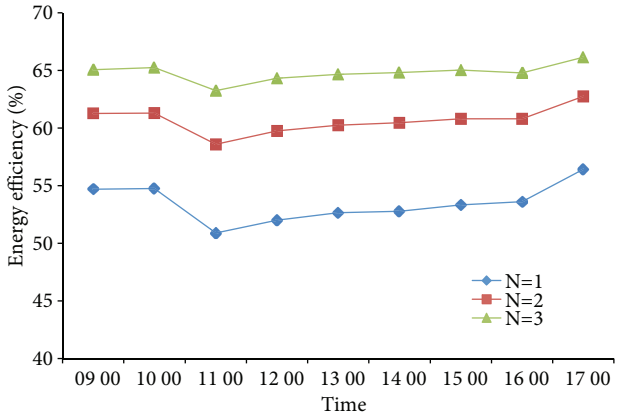

Figure 14. Variation in energy efficiency for different numbers of glass covers (L = 1.9 m, h_e = 0.01 m, W = 0.9 m, V = 2 m s^{-1}, D = 0.043 m).

The maximum outlet temperature was 333.8 K for the triple glass cover at 1100 hours. Mean outlet temperatures were 325.7, 327.3, and 328.2 K for single, double, and triple glass covers, respectively. The collector had the maximum mean outlet temperature for the triple glass cover.

The maximum energy efficiency was 66.1% for the triple glass cover at 1700 hours. Mean energy efficiency was 53.4%, 60.6%, and 64.8% for single, double, and triple glass covers, respectively. The collector had the maximum mean energy efficiency for the triple glass cover.

The maximum exergy efficiency was 3.89% for the triple glass cover at 1100 hours. Mean exergy efficiency was 2.07%, 2.54%, and 2.83% for single, double, and triple glass covers, respectively. The collector had the maximum mean exergy efficiency for the triple glass cover.

Outlet temperature, and energy and exergy efficiencies were also investigated for different lengths of the collector, i.e. 1, 1.5, 2, 2.5, and 3 m. The results are shown in Figures 16–18. Outlet temperature increased but energy efficiency decreased with the increase in the length of the collector. Exergy efficiency increased with the increase in the length of the collector but it decreased gradually after 1100 hours for each length.

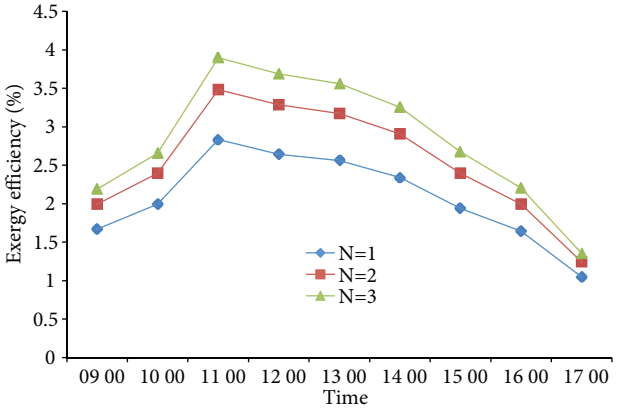

Figure 15. Variation in exergy efficiency for different numbers of glass covers (L = 1.9 m, h_e = 0.01 m, W = 0.9 m, V = 2 m s^{-1}, D = 0.043 m).

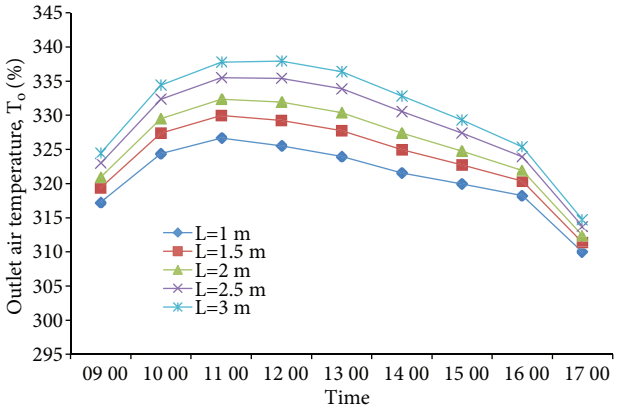

Figure 16. Variation in outlet temperature for different lengths of the collector (h_e = 0.01 m, W = 0.9 m, V = 2 m s^{-1}, D = 0.043 m, N = 1).

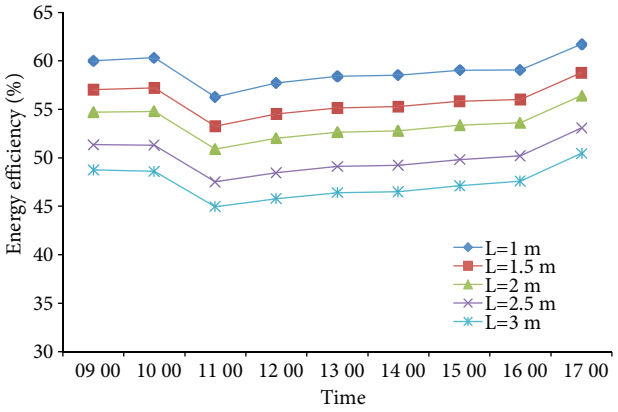

Figure 17. Variation in energy efficiency for different lengths of the collector (h_e = 0.01 m, W = 0.9 m, V = 2 m s^{-1}, D = 0.043 m, N = 1).

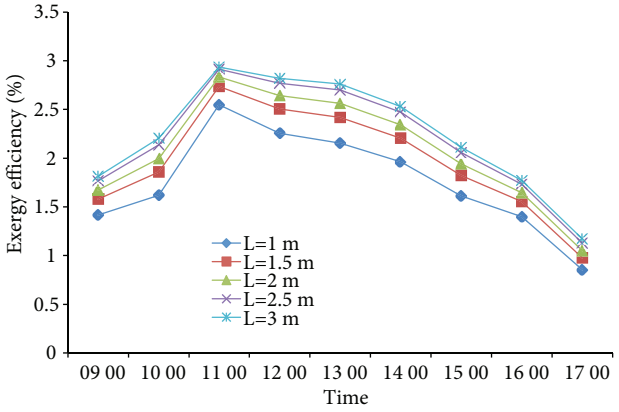

Figure 18. Variation in exergy efficiency for different lengths of the collector (h_e = 0.01 m, W = 0.9 m, V = 2 m s^{-1}, D = 0.043 m, N = 1)

The maximum outlet temperature was 337.9 K for the length of 3 m at 1200 hours. Mean outlet temperatures were 320.8, 323.6, 325.7, 328.4, and 330.3 K for the length of 1, 1.5, 2, 2.5, and 3 m, respectively. The collector had the maximum mean outlet temperature for the length of 3 m.

The maximum energy efficiency was 61.7% for the length of 1 m at 1700 hours. Mean energy efficiency was 59.0%, 55.8%, 53.4%, 50.0%, and 47.3% for the length of 1, 1.5, 2, 2.5, and 3 m, respectively. The collector had the maximum mean energy efficiency for the length of 1 m.

The maximum exergy efficiency was 2.93% for the length of 3 m at 1100 hours. Mean energy efficiency was 1.75%, 1.96%, 2.07%, 2.18%, and 2.23% for the length of 1, 1.5, 2, 2.5, and 3 m, respectively. The collector had the maximum mean energy efficiency for the length of 3 m.

To improve the overall efficiency of the system, the irreversibilities should also be reduced along with the application of optimum design parameters.

6. Conclusions

Such heaters are implemented in many applications such as space heating, and drying for industrial and agriculture purposes, which require low to moderate temperature below 60 °C. In this study outlet temperatures and the collector efficiencies obtained both experimentally and theoretically were compared. The collectors were tested experimentally for the tilt angle of 35° and 2 m s^{-1} air velocity and mean outlet, absorber plate, and bottom plate temperature were 346.8, 370.6, and 350.7 K, respectively, between 0900 and 1700. The algorithm was improved with energy and exergy equations and run using FORTRAN codes and the results of this theoretical study were compared with those of the experimental study for validation. The results were found compatible with the experiments.

Simulation was also performed to investigate the outlet temperature, and energy and exergy efficiencies for different values of the parameters as follows: airflow velocity of 1, 2, 3, and 4 m s^{-1}; airflow duct height of 0.01, 0.1, 0.5, 1, 2, 3, and 4 cm; number of glass covers: single, double, and triple form; and length of the collector of 1, 1.5, 2, 2.5, and 3 m. The results showed that the collector had the maximum mean outlet temperature for the airflow velocity of 1 m s^{-1}, duct height of 0.001 m, the triple glass cover, and length of 3 m; the maximum mean energy efficiency for the airflow velocity of 4 m s^{-1}, duct height of 0.04 m, the triple glass cover, and length of 1 m; the maximum mean exergy efficiency for the airflow velocity of 1 m s^{-1}, duct height of 0.005 m, the triple glass cover, and length of 3 m. It is recommended to focus on the minimum exergy values for the design improvements of solar collectors. Exergy analysis provides information about the locations of the inefficiencies, unlike energy analysis.

Nomenclature

A_c	area of absorber plate (m^2)
A	cross-sectional area of the airflow duct (m^2)
c_p	specific heat of air (J kg^{-1} K^{-1})
D	airflow duct height (m)
h_{cpf}	convective heat transfer coefficient between the flowing air and the absorber plate (W m^{-2} K^{-1})
h_{cbf}	convective heat transfer coefficient between the flowing air and the bottom plate, (W m^{-2} K^{-1})
h_{rpb}	radiative heat transfer coefficient between the absorber plate and the bottom plate, (W m^{-2} K^{-1})
F_R	heat removal factor
F'	heat efficiency factor
G_T	solar radiation on the collector plane, (W m^{-2})
h	enthalpy of air (kJ kg^{-1})
h_e	collector side wall height (m)
h_w	wind heat transfer coefficient (W m^{-2} K^{-1})
I	irreversibility (kW)
k	thermal conductivity of insulation (W m^{-2} K^{-1})
L	length of the collector (m)
m	mass flow rate (kg s^{-1})
N	number of glass covers
Nu	Nusselt number
Q_u	useful heat gain (W)
Q_s	solar energy absorbed by the collector absorber surface (kW)
Pr	Prandtl number
Re	Reynolds number
s	entropy of air (kJ kg^{-1} K^{-1})
T_a	ambient temperature (K)
t_b	thickness of bottom insulation (m)
t_e	thickness of edge insulation (m)
T_{fm}	mean flow temperature (K)
T_i	inlet air temperature (K)
T_o	outlet air temperature (K)
T_{pt}	estimated mean plate temperature (K)
T_{pm}	mean plate temperature (K)
U_L	overall loss coefficient (W m^{-2} K^{-1})
V	fluid velocity (m s^{-1})
V_r	wind velocity (m s^{-1})
W	width of the duct (m)
η_I	energy efficiency (%)
η_{II}	exergy efficiency (%)

Greek symbols

ε	emissivity
σ	Stefan–Boltzmann coefficient (5.67×10^{-8} W m^{-2} K^{-4})
β	tilt angle (°)
μ	dynamic viscosity of air (kg m^{-1} s^{-1})

λ	thermal conductivity of insulation material (W m^{-1} K^{-1})
ρ	density of air (kg m^{-3})
$\tau\alpha$	transmittance-absorptance product

Subscripts

b	bottom
e	edge
g	glass cover
p	plate

Acknowledgment

The authors are grateful to the Scientific Research Project Units of Akdeniz University for funding.

References

[1] Tchinda R. A review of the mathematical models for predicting solar air heaters systems. Renew Sust Energ Rev 2009; 13: 1734–1759.

[2] Hegazy AA. Performance of flat plate solar air heaters with optimum channel geometry for constant/variable flow operation. Energ Convers Manage 2000; 41: 401–417.

[3] Varun S. Thermal performance optimization of a flat plate solar air heater using genetic algorithm. Appl Energ 2010; 87: 1793–1799.

[4] Torres-Reyes E, Navarrete-González JJ, Zaleta-Aguilar A, Cervantes-de Gortari JG. Optimal process of solar to thermal energy conversion and design of irreversible flat-plate solar collectors. Energy 2003; 28: 99–113.

[5] Torres-Reyes E, Navarrete-González JJ, Cervantes-de Gortari JG. Thermodynamic optimization as an effective tool to design solar heating systems. Energy 2004; 29: 2305–2315.

[6] Gupta MK, Kaushik SC. Exergetic performance evaluation and parametric studies of solar air heater. Energy 2008; 33: 1691–1702.

[7] Luna D, Jannot Y, Nadeau JP. An oriented-design simplified model for the efficiency of a flat plate solar air collector. Appl Therm Eng 2010; 30: 2808–2814.

[8] Koyuncu T. Performance of various design of solar air heaters for crop drying applications. Renew Energ 2006; 31: 1073–1088.

[9] Dhiman P, Thakur NS, Kumar A, Singh S. An analytical model to predict the thermal performance of a novel parallel flow packed bed solar air heater. Appl Energ 2011; 88: 2157–2167.

[10] Karwa R, Chauhan K. Performance evaluation of solar air heaters having v-down discrete rib roughness on the absorber plate. Energy 2010; 35: 398–409.

[11] Varol Y, Öztop HF. A comparative numerical study on natural convection in inclined wavy and flat-plate solar collectors. Build Environ 2008; 43: 1535–1544.

[12] Bergman TL, Lavine AS, Incropera FP, Dewitt DP. Fundamentals of Heat and Mass Transfer. 7th ed. New York, NY, USA: Wiley; 2011.

[13] Hsieh JS. Solar Energy Engineering. Upper Saddle River, NJ, USA: Prentice Hall; 1986.

[14] Duffie JA, Beckmann WA. Solar Engineering of Thermal Processes, 2nd ed. USA: New York, NY, US: Wiley; 1991.

[15] Alta D, Bilgili E, Ertekin C, Yaldız O. Experimental investigation of three different solar air heaters: energy and exergy analyses. Appl Energ 2010; 87: 2953–2973.

[16] Languri EM, Ganji DD. Thermal aspects of solar air collector. Heat transfer - mathematical modelling, numerical methods and information technology. In: Belmiloudi A, editor. InTech; 2011. pp. 642. Available from: http://www.intechopen.com/books/heat-transfer-mathematical-modelling-numerical-methods-and-information-technology/thermal-aspects-of-solar-air-collector.